Heavy-Lift Airship Dynamics

Mark B. Tischler,* Robert F. Ringland,† and Henry R. Jex‡
Systems Technology, Inc., Hawthorne, California

A nonlinear, multibody, 6-degrees-of-freedom digital simulation has been developed to study generic heavy-lift airship (HLA) dynamics and control. The slung-payload and flight control system models are described, and a review of the aerodynamic characteristics of an example vehicle is presented. Trim calculations show the importance of control mixing selection, and suggest performance deficiencies in crosswind stationkeeping for the unloaded example HLA. Numerically linearized dynamics of the unloaded vehicle exhibit a divergent yaw mode and an oscillatory pitch mode whose stability characteristic is sensitive to flight speed. The vehicle with slung payload shows significant coupling of the payload modes with those of the basic HLA. The accuracy of decoupled linearized models is sensitive to the size of dynamic excursions and the vehicle loading condition. A considerable improvement in the vehicle's stability and response is shown using a simple, multiaxis closed-loop control system operating on the rotor and propeller blade pitch controls.

Nomenclature

h = altitude
L,M,N = aerodynamic moments about x,y,z reference axes, respectively
p,q,r = components of angular velocity about x,y,z reference axes, respectively
s = Laplace transform operator
$1/T_s$, $1/T_h$, $1/T_{sy_1}$, $1/T_{sy_2}$ = surge, heave, and sway/yaw inverse time constants, respectively (time-to-half-amplitude = $0.693T$; $T = T_s$, T_h, T_{sy_1}, T_{sy_2})
u,v,w = components of velocity along x,y,z axes, respectively
x, y, z = orthogonal, right-hand coordinate axes; positive z is down
X,Y,Z = aerodynamic forces along the x,y,z axes, respectively
α = tail angle of attack $\equiv \tan^{-1}(w_{t_a}/u_{t_a})$
α_1 = value of α for stall or vortex breakdown
α_2 = value of α for start of predominantly cross-flow regime
β = tail angle of sideslip, $\beta \equiv \tan^{-1}(v_{t_a}/u_{t_a})$ (nonstandard definition)
δ_u, δ_v, δ_w, δ_θ, δ_ϕ, δ_ψ = surge, sway, heave, pitch, roll, and yaw control deflections, respectively
ζ_p, ζ_r = pitch and roll mode damping ratios, respectively
ζ_{lat}, ζ_{lon} = lateral and longitudinal slung-payload pendulum mode damping ratios, respectively
ζ_{y_v} = yaw vibration slung-payload mode damping ratio
$\zeta_{h_v}, \zeta_{r_v}, \zeta_{p_v}$ = heave, roll, and pitch slung-payload vibration mode damping ratios, respectively
ω_p, ω_r = pitch and roll mode undamped natural frequencies, respectively
ω_{lat}, ω_{lon} = lateral and longitudinal slung-payload pendulum mode natural frequencies, respectively
ω_{y_v} = yaw vibration slung-payload mode natural frequency
ω_{h_v}, ω_{r_v}, ω_{p_v} = heave, roll, and pitch slung-payload vibration mode natural frequencies, respectively

Subscripts

a = apparent, relative to local airmass
c = command
c.g. = center of gravity
c.v. = center of volume
h = hull
o = reference value
p = payload
t = tail

Superscript

$(\dot{\ })$ = time derivative with respect to nonrotating axes

Received Sept. 28, 1981; revision received May 25, 1982. Published by the American Institute of Aeronautics and Astronautics with permission.

*Staff Engineer, Research (presently, Aerospace Engineer, Aeromechanics Laboratory, U.S. Army Research and Technology Laboratories (AVRADCOM), Ames Research Center, Moffett Field, Calif.). Member AIAA.

†Principal Specialist (presently, Senior Technical Specialist, Northrop Advanced Systems Division, Los Angeles, Calif.). Associate Fellow AIAA.

‡Principal Research Engineer. Member AIAA.

I. Introduction

RECENT feasibility studies[1-3] have shown that the heavy-lift hybrid airship (HLA) is an efficient and cost-effective vehicle for lifting, transporting over short distances (200 km), and positioning massive loads (typically up to 100 tons). These studies suggest that because of its economic advantages the HLA may serve in an important future role in the areas of logging, container ship off-loading, remote site supply, and coastal patrol.

While many economic studies are found in the literature, only limited analytical treatment of the engineering problems associated with operation of these vehicles in their intended roles has been published.[4,5] The studies of conventional, and more recently heavy-lift, airship dynamics and control have used the classical, linearized, small perturbation approaches. However, the validity of using such techniques for the study of the HLA, a relatively new class of vehicle, has yet to be established.

Unlike the lighter-than-air vehicles of the past, the heavy-lift airship will have large thrust-to-weight ratios and low fineness ratios. As a result, significant nonlinear rotor/hull aerodynamic interactions, not considered a problem in classic airships, have been reported.[6,7] Also, unlike its predecessors, the HLA will typically be used in missions requiring precise control through flight regimes encompassing large and rapid changes of speed, incidence, and inertial properties. The response of these vehicles to gusty environments has become

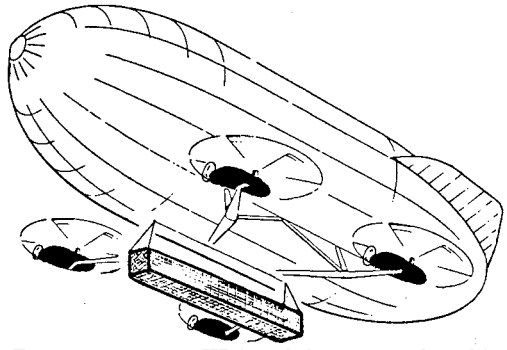

Fig. 1 Example quadrotor HLA and slung-payload used in present simulation.

an important issue, receiving only limited analytical treatment in the past.[8-10] Historically, the lack of control over gust-induced motions has proven the undoing of many dirigibles and blimps. The modern HLA, with its greatly increased control power (rotors and propellers), has the challenge of and potential for solving these traditional problems.

An accurate, nonlinear, non-real-time 6-degrees-of-freedom (DOF) simulation to investigate the technological problems of the buoyant quadrotor (BQR) concept (Fig. 1). Specific areas of concern already noted are aerodynamics, flight dynamics, and flight controls. The simulation is intended for use as a basic design synthesis and analysis tool for evaluation of competing designs.

The example configuration, used for software development and simulation demonstration, is representative of a class of low fineness ratio, quadrotor HLAs having small fins and designed for efficient low speed cruise and hover flight. The assumed geometric and inertial properties of the loaded and unloaded vehicle are given in Table 1.

The simulation provides the capability to investigate generic properties and basic vehicle characteristics. It also permits the evaluation of the relative importance of aerodynamic and dynamic nonlinearities. Throughout the program, emphasis was placed on determining dominant effects and obtaining gross loads and motions, using models based on uniformly valid first approximations to a variety of effects. Also recognized was the need to minimize input data requirements to facilitate design tradeoff studies.

A comprehensive description of the simulation models and typical results was given in an extensive paper at the 1981 AIAA Lighter Than Air (LTA) Conference.[11] The present paper highlights the discussion of the flight control system model and example vehicle aerodynamics with emphasis

Table 1 Geometric and inertial properties of the loaded and unloaded BQR

Hull		
Length		240 ft
Diameter		103 ft
Volume		1.5×10^6 ft^3
Tail area		2520 ft^2
Weight		8.89×10^4 lb
Lift propulsion unit (LPU)		
Rotor diameter		56 ft
Propeller diameter		13 ft
Engine horsepower (one per LPU)		1524 hp
Weight (each LPU)		9×10^3 lb
Composite vehicle	Unloaded	Loaded
Weight (lb)	125,000	165,000
Buoyancy ratio	0.92	0.70

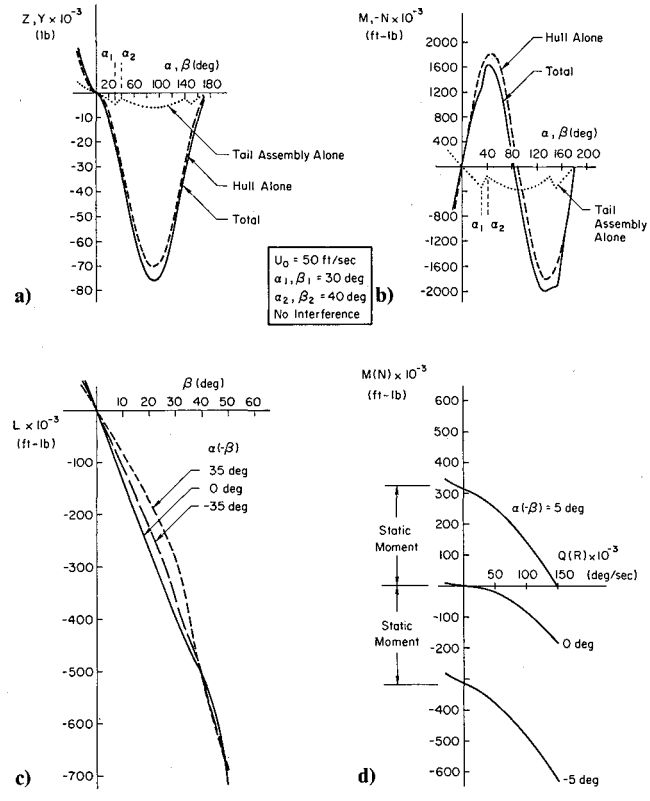

Fig. 2 Samples of simulated forces and moments for example case of Fig. 1: a) Z or Y force; b) static pitching, yawing moment; c) static rolling moment; d) damping moment, hull alone.

placed on the presentation of performance and dynamic characteristics. The slung-payload model is described, and a preliminary analysis of the coupled vehicle/payload dynamics is presented. The vehicle description in Table 1 has been corrected from the original paper.[11]

II. Description of Simulation

This section will review the simulation capabilities and describe the aerodynamic, slung-payload, and flight control system models. The aerodynamic characteristics of the example configuration are presented to provide insight into the physics of the vehicle dynamics discussed in a later section. The results presented here employ the basic (noninterference) aerodynamic models.

Simulation Capabilities

The NASA/STI simulation is composed of four computer programs: vehicle, payload, vehicle/payload, and mooring.

Simulation capabilities include the calculation of trim conditions (operating points) and the associated operating point equations of motion; normal mode response parameters; and large amplitude (nonlinear) motion time histories. The trim solution (unmoored) is an iterative calculation of control positions required to null vehicle (and payload) accelerations at selected orientations, velocities, and local wind directions. This capability is very useful for identifying control power requirements, operational envelopes, and performance tradeoffs. Small perturbations about selected trim points are used to generate numerically the open-loop (i.e., controls-fixed) system characteristic matrix, and the control and gust input matrices for linear systems analyses. These matrices can be used to evaluate the vehicle open-loop transfer functions for flight control system synthesis, including time and frequency responses.

Fully nonlinear responses of the HLA and payload to a variety of control system commands and gust inputs are generated for open- and closed-loop studies. Control system

commands, feedbacks, gains, and limits are determined from user inputs. Over 1000 states, component loads, and other dependent variables can be accessed at each time step and plotted or tabulated as desired. This capability can provide valuable insight into the importance of many nonlinear aerodynamic and dynamic terms.

The following subsections present summaries of the aerodynamic, slung-payload, and flight control system models. The reader is referred to detailed descriptions[11-13] of the aerodynamics models, dynamic equation formulation, and software architecture.

Steady Aerodynamics Model of Example Vehicle

The quasisteady aerodynamic characteristics for the bare hull and hull/tail assembly of the example configuration of Fig. 1 are presented in Fig. 2 for a constant flight speed of 50 ft/s. The hull properties are assumed equal in pitch or yaw axes, and the tail-on-hull properties for the 45-deg "vee-tail" are assumed to be the same in pitch or yaw, except for the rolling moment. Semiempirical methods[14-17] were used to estimate the basic aerodynamic characteristics. The static $Z(Y)$ force (Fig. 2a) is seen to be dominated by the bare hull, as a result of the small tail exposed area. The static pitching (yawing) moment characteristics about the center of volume (Fig. 2b) show that the small stabilizing tail contribution is completely overridden by the large unstable hull contribution, thereby rendering the static vehicle aerodynamically unstable (metacentric stability not included). The present test case, which has a "vee-tail," exhibits large negative rolling moments due to sideslip (postive dihedral effect). Figure 2c shows significant nonlinearities in the model for angles of attack of $+35$ and -35 deg, owing to the assumed breakdown of attached flow in the stall transition regimes. The hull-alone damping characteristics for axial and nonaxial flight are presented in Fig. 2d. The offsets in moments at zero angular rate $(q,r=0)$ are due to the static hull moment characteristics. The significant increase in damping moment with angular rate for non-zero α or β results from the w_{h_a} and v_{h_a} dependency in the hull damping model.[11]

Slung-Payload Model

A slung-payload model was developed in order to study the generic problems of hull/payload dynamic coupling and performance. A versatile sling geometry was implemented which allows the connection of the payload and hull by four (or less) elastic cables. Attach points on the hull and payload are user-selected to facilitate tradeoff studies among various sling configurations (e.g., pendant, "inverted vee," etc.). Each cable is described in terms of spring stiffness and damping constants, with sling mass and aerodynamic properties neglected.

For the present simulation, a simple quasisteady payload aerodynamics model was implemented which is suitable for trim performance and low speed dynamic analyses of high density containers. This model, which is essentially identical to the hull (tail-off) quasisteady aerodynamic model, accounts for potential flow moments, and viscous drag and damping loads. The model neglects the complex discontinuities (hysteresis, separation bubbles, etc.) and unsteady aerodynamics known to be significant for detailed assessment of stability boundaries and full-scale flight correlation.[18] Future simulation users can easily adapt the present aerodynamics model for specific payload configurations should a detailed assessment be required.

The payload used as an example is a rectangular cargo container suspended by an "inverted-vee" sling. The container is suspended 3-deg nose-down for improved dynamic stability characteristics.[18] The payload and sling geometry is shown in Fig. 1. The stiffness constant is typical for sling cables and was obtained from Sampath.[18] The damping constant was selected to yield a heave vibration mode damping ratio of about 0.2. As indicated in Table 1, the payload weight is 20 tons. Aerodynamic parameters were obtained from cargo container wind tunnel data.[18]

Flight Control System

The flight control system implemented in the simulation exercises control over all 6 deg of hull motion freedom. It functions to maintain trimmed flight conditions in the presence of disturbances and to execute maneuver commands.

Control Mixing

With four lift-propulsion units (LPUs), each having a rotor and a propeller, and three fin deflection controls, there are a total of 27 possible control points. Sixteen of these are active in the example HLA, four on each of the four LPUs. These are the propeller and rotor collectives, and the rotor lateral and longitudinal cyclics. Each of these is effective between user-set limits corresponding to mechanical limits at the control surface. The remaining control points are the rotor and propeller rpms, which are fixed at user-set values in the present simulation. The three fin deflections are fixed at zero.

The simulation incorporates the software equivalent of a "mixer box" to link the active control surfaces into six approximately orthogonal control input points, one for each degree of freedom. An input to one of these points is equivalent to commanding an acceleration in one of the 6DOF. The six linked control points established by the mixer box are used to compute the trim operating points for the vehicle, for calculating linearized control response derivatives, and for simulation flight control when computing time histories.

In the present model, the six acceleration command points are related to the linked control surfaces as follows: pitch, (δ_θ)—fore-and-aft differential rotor collectives; roll (δ_ϕ)—side-to-side differential rotor collectives; yaw (δ_ψ)—side-to-side differential propeller collectives and differential rotor longitudinal cyclics; surge (δ_u)—propeller collective and rotor longitudinal cyclics; sway (δ_v)—rotor lateral cyclics; heave (δ_w)—rotor collectives.

The scheme mixes rotor longitudinal cyclics and propeller collectives to assure adequate control power for hovering with and without a payload, i.e., over a wide range of operating rotor thrust conditions. The mixing ratio is user-selected. The lateral cyclics are used exclusively for side force (sway) control because this axis is most control power limited—the propellers are directed forward in the example HLA.

Flight Control Loops

Upstream of the mixer-box are the individual flight control loops, one for each of the acceleration control points. The pitch control loop, a typical example, is shown in Fig. 3. It incorporates feedback of pitch attitude and body axis pitch rate and contains proportional and integral paths in the forward loop. The attitude and body axis rate feedbacks provide command response and stability augmentation, while the forward loop integrator (initialized by the trim condition calculation at the start of the run) insures zero steady-state attitude error. The user determines the gain choices based upon analysis of the control requirements. The output is limited by a user-set value as is the integral term. The output limit prevents the pitch channel from using all the control authority that might otherwise be available at one or more of the rotor collectives. The integrator limit similarly prevents the trim term from saturating the pitch control channel; the combined proportional-plus-derivative signal can always influence the pitch control, δ_θ. Upon encountering the limit, the integrator input is removed until it changes sign, when it is restored.

The control-augmented airframe constitutes an attitude-command/attitude-hold system, which is a favorable characteristic for low speed and hovering flight operations.[19] Such a system, while not highly maneuverable for "up and

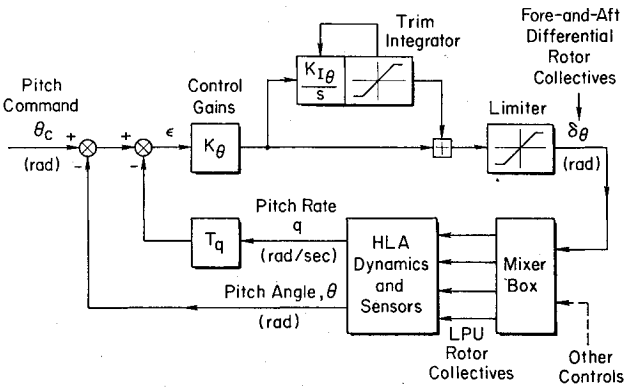

Fig. 3 Block diagram for pitch control loop.

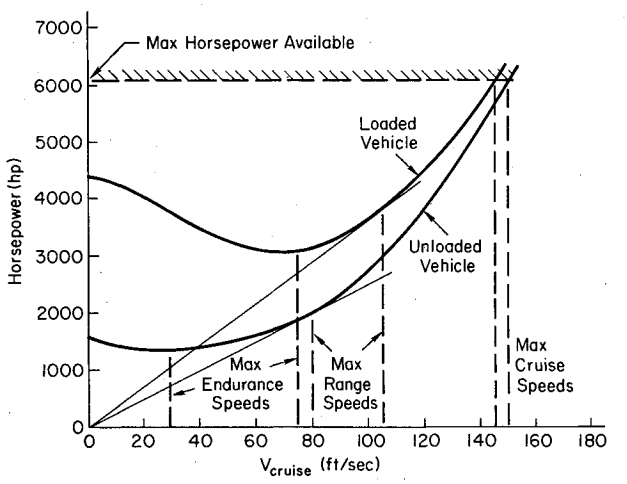

Fig. 4 Power requirements for trimmed forward flight.

away" flying, allows for limited periods of unattended operation in controlling pitch attitude which will likely be required during payload pickup and drop, especially in gusty environments.

The simulation software organization is structured so as to confine control system changes to a limited number of subroutines, thereby making it easy for the user to reprogram for a particular HLA configuration under evaluation. Among the parameters suited for study using the flight control system model are requirements for control power as a function of task and flight condition; control gain and limit schedules; crossfeeds between channels (e.g., for turning flight in cruise); and sensor location and orientation.

III. Typical Simulation Results

This section presents some results of the simulation to illustrate the program functions and to show the motion dynamics for one class of HLA, the example configuration of in Fig. 1.

Trimmed Flight Conditions

A series of trimmed flight conditions covering a wide range of speed and incidences was computed in order to investigate the control authority requirements and flight envelope boundaries for both the unloaded and loaded configurations. The example payload aerodynamic forces are very small compared to its weight, and so the resulting effects on performance were found to be correspondingly small (i.e., less than 2% at 44 ft/s). For the trim analysis given here, the payload aerodynamics were neglected. Payload aerodynamics and sling dynamics *are* considered in the coupled vehicle/payload analysis discussed later.

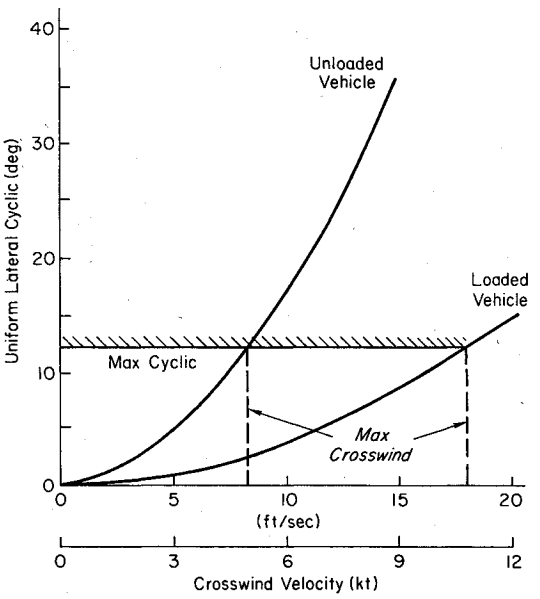

Fig. 5 Trimming for hover in a steady crosswind.

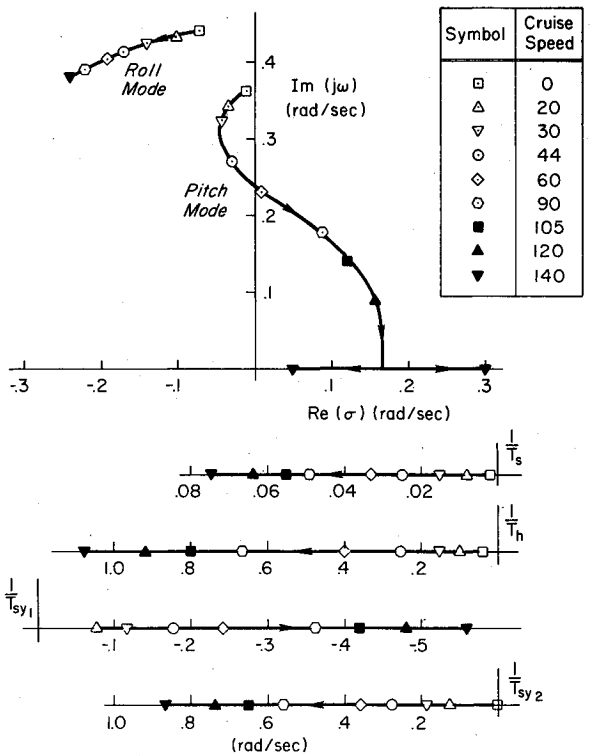

Fig. 6 Migration of unloaded HLA modes with cruise speed.

Power Requirements

Figure 4 shows the total vehicle power requirements as a function of sea-level axial flight speed for the unloaded and loaded configurations. Power is required at hover, even when unloaded, because the buoyancy ratio is less than unity. Based on a total available power rating of 6100 hp, the maximum unloaded cruise speed is 152 ft/s (103 mph), compared to 145 ft/s (99 mph) for the loaded vehicle.

These results show the importance of the longitudinal control crossfeed between propeller collective and rotor pitch cyclic. If the longitudinal crossfeed gain is kept the same for the loaded and unloaded configurations, as it was in the present case, rotor thrust contributes a greater proportion of cruise propulsion when the vehicle is loaded. Rotors, as a result of their large disk areas, are inherently more efficient

for low speed cruise propulsion than are propellers. Therefore the power requirements for the loaded and unloaded vehicles are essentially the same at maximum speed. Scheduling the crossfeed gain to optimize rotor and propeller usage for changing loading conditions will greatly improve overall vehicle performance.

The speed for maximum range and speed for maximum endurance, critical design parameters for HLAs, are seen to be 80 and 30 ft/s for the unloaded and 105 and 75 ft/s for the loaded vehicle, respectively. These parameters can be tailored to design specification by systematically exercising the simulation trim function for a range of configurations.

Crosswind Hover

The operation of HLAs in crosswind hover conditions is an important design consideration. Figure 5 presents the required uniform rotor lateral cyclic (δ_v) for upright trim (zero roll angle) as a function of crosswind velocity for the loaded and unloaded vehicle. For a typical lateral cyclic limit of ± 12 deg, this figure indicates a maximum crosswind capability of 8 ft/s (4.7 knots) for the unloaded vehicle. The loaded configuration, which trims with larger rotor thrusts, has a crosswind capability of 18 ft/s (10.7 knots). Trimming at nonzero roll angles would generate larger lateral rotor forces; however, significant roll control (δ_φ) would be required to offset the vehicle metacentric rolling moment, and/or a more complex load-handling suspension cable control system would be required to allow steady roll angles under load.

Small Perturbation Dynamics—Vehicle Alone

The coefficients for the linearized, small perturbation equations of motion were numerically determined for a number of trimmed, controls-fixed, flight conditions without a payload. Additional cases were calculated for a rigidly attached payload, the slung payload alone, and the HLA with slung payload. The characteristic roots of the system, each being associated with a particular dynamic mode of response, were calculated for the various flight conditions.

In describing the characteristic modes of response, we use a shorthand notation for Laplace transform factors. Thus $(1/T)$ denotes the factor $(s+1/T)$, while $[\zeta, \omega]$ denotes $[s^2+2\zeta\omega s+\omega^2]$. These common metrics in the frequency domain are related to the common time domain metrics as follows:

$$\text{Time-to-half-amplitude} = 0.693T \quad \text{(real roots)}$$

$$= 0.693/\zeta\omega \quad \text{(complex roots)}$$

$$\text{Complex root location} = -\zeta\omega \pm j\omega\sqrt{1-\zeta^2}$$

Table 2 summarizes the characteristic roots for several cases at 44 ft/s. This condition is representative of blimp-like operations. A discussion of these results is presented below.

The *unloaded* vehicle (Table 2, line a) exhibits the following five basic modes.

Surge Subsidence $(1/T_s)$

This stable mode is a 1DOF motion, comprising variations in axial speed ($u_{h_{c.g.}}$). About 50% of the surge damping arises from vehicle drag, while the remaining portion arises from rotor and propeller effects. This motion is largely decoupled from the other modes because M_u and Z_u are small in this flight condition.

Heave Subsidence $(1/T_h)$

This stable mode is predominantly composed of vertical motion and derives most of its damping from the rotors. The rotor flapping dynamics induce some coupling between heave, sway, and surge motions, the modal response ratios being

$$\left| u_{h_{c.g.}} : v_{h_{c.g.}} : w_{h_{c.g.}} \right|_{1/T_h} = \left| 0.14 : 0.2 : 1 \right|$$

Significant coupling between the heave and pitch motions, measured in terms of the hull pitch angle to hull angle-of-attack modal ratio:

$$\left| \theta_h : \alpha_{h_{c.g.}} \right|_{1/T_h} = \left| 0.7 : 1 \right|$$

arises from the tail lift response to vertical velocity. Barring this coupling, the HLA heave mode resembles the heave mode exhibited by V/STOL aircraft.[20]

Pitch Oscillation (ζ_p, ω_p)

The oscillatory pitch mode comprises variations in $u_{h_{c.g.}}$, $w_{h_{c.g.}}$, and θ_h. The eigenvector phasing shows that θ_h variations lead $w_{h_{c.g.}}$ and $u_{h_{c.g.}}$ by 25 and 273.3 deg, respectively. Although somewhat resembling the classical aircraft phugoid mode in frequency and damping, the present motion exhibits large changes in hull angle of attack,

$$\left| \alpha_{h_{c.g.}} : \theta_h \right|_{\omega_p} = \left| 0.55 : 1 \right|$$

Further, the frequency of oscillation (ω_p) is determined by the metacentric height (of c.v. above c.g.), the static aerodynamic pitch instability [effective M_α of the total vehicle is positive (Fig. 2b)], and the total vehicle effective pitch inertia. The light oscillatory damping (ζ_p) is provided by the hull, tail, and rotors. For the 44-ft/s flight condition, the rotors generate about 70% of the vehicle effective pitch damping.

Coupled Sway-Yaw $(1/T_{sy_1}, 1/T_{sy_2})$

This mode comprises coupled variations in side velocity ($v_{h_{c.g.}}$) and yaw angle (ψ_h). The modal instability arises from the unstable static aerodynamic yawing moment characteristic of the hull/tail assembly (Fig. 2b). The unstable root $(1/T_{sy_1})$ and stable root $(1/T_{sy_2})$ locations depend on the yawing

Table 2 Characteristic roots for the unloaded and loaded vehicle at 44 ft/s (30 mph)

Vehicle modes	Surge $(1/T_s)$	Heave $(1/T_h)$	Pitch $[\zeta_p, \omega_p]$	Sway-yaw $(1/T_{sy_1})$ $(1/T_{sy_2})$	Roll $[\zeta_r, \omega_r]$
a) Vehicle unloaded	(0.0245)	(0.253)	[0.107, 0.273]	(−0.175) (0.279)	[0.371, 0.447]
b) Vehicle loaded	(−0.0076)	(0.220)	[0.137, 0.340]	(−0.167) (0.267)	[0.298, 0.498]
c) Coupled vehicle/ slung load	(−0.0035)	(0.220)	[0.142, 0.330]	(−0.167) (0.266)	[0.320, 0.524]

Payload modes	Lateral pendulum $[\zeta_{lat}, \omega_{lat}]$	Longitudinal pendulum $[\zeta_{lon}, \omega_{lon}]$	Yaw vibration $[\zeta_{y_v}, \omega_{y_v}]$	Heave vibration $[\zeta_{h_v}, \omega_{h_v}]$	Roll vibration $[\zeta_{r_v}, \omega_{r_v}]$	Pitch vibration $[\zeta_{p_v}, \omega_{p_v}]$
d) Slung load only	[0.003, 1.112]	[0.008, 1.285]	[0.084, 5.004]	[0.187, 9.338]	[0.304, 15.600]	[0.332, 16.592]
e) Coupled vehicle	[−0.004, 1.180]	[0.007, 1.429]	[0.085, 5.059]	[0.200, 10.803]	[0.306, 15.632]	[0.335, 16.798]

moment characteristics and the lateral drag and rotor damping. The coupled yaw-sway mode is similar to the unstable spiral mode in conventional aircraft.

Roll Oscillation (ζ_r, ω_r)

The stable oscillatory roll mode is a well-damped 1DOF "pendulum motion" composed of variations in side velocity ($v_{h_{c.g.}}$) and roll angle (ϕ_h). The modal response ratios indicate that the effective center of rotation is 3 ft below the hull center of volume and above the unloaded vehicle's composite c.g., due largely to apparent mass and inertia effects. The natural frequency (ω_r) is controlled by the metacentric height and effective roll inertia, while the damping (ζ_r) is generated by the rotors and tail.

Dynamic modes of HLAs and classical airships have been calculated by previous authors. The HLA longitudinal analysis completed by Nagabhushan and Tomlinson[5] showed the existence of the surge, heave, and pitch oscillatory modes, resembling those presented here. The lateral and longitudinal open-loop results presented by Delaurier and Schenck[4] are in correspondence with the five modal responses discussed here. Although specific damping ratios and frequencies vary (depending on the configuration under study), the mode shapes and relative eigenvalue locations are very similar.

Effect of Payload on System Dynamics

The loaded vehicle (rigidly attached payload) has the characteristic roots shown in Table 2, line b. The added payload weight results in a sizeable increase in the trim rotor thrust and related rotor blade coning and flapping. This produces significant coupling between the longitudinal and lateral-directional degrees of freedom. The surge mode now has substantial sway motion and has become slightly unstable. Except for minor changes in the oscillatory frequencies due to increased metacentric height (above the lowered c.g.) the remaining vehicle modes are essentially unchanged from the unloaded values in line a.

The vehicle/slung-load configuration has eleven characteristic modes of response. The first five of these correspond to those of the basic vehicle. These basic vehicle modes of response induce in-phase payload motion of almost equal magnitude. For example, the (coupled) vehicle pitch oscillation modal ratios are

$$\left|\alpha_{h_{c.g.}} : \theta_h : \theta_p \right|_{\omega_p} = \left|0.57 : 1 : 0.93\right|$$

This strong coupling into payload motions is due to the sling geometry which with inverted vee slings both forward and aft on the payload (Fig. 1) causes it to move with the hull. The coupled system responds as a single rigid body, with nearly the same modal characteristics as the loaded vehicle (rigidly attached payload) case. The associated coupled system roots are shown in Table 2, line c, and very closely match those of the loaded vehicle, as expected.

The characteristic roots of the slung-payload-only system (in isolation) are listed in Table 2, line d, and reveal six modes of response. The two lowest-frequency modes are associated with longitudinal [ζ_{lon}, ω_{lon}] and lateral [ζ_{lat}, ω_{lat}] pendulum modes. These have very low damping ratios because of the small aerodynamic damping in this flight condition. The next-highest frequency mode [ζ_{y_v}, ω_{y_v}] is associated with yawing motions of the payload. Here the arrangement of the sling is such that cable spring force and damping contribute substantially to a higher frequency and damping ratio. The three highest-frequency vibration modes are dominated by the cable spring and damping constants.

The vehicle/slung-load modes, which correspond to the isolated slung-payload modes, are presented in Table 2, line e. A comparison of the results (lines d and e) shows that the characteristic roots are essentially unaffected. However, the payload motion now induces significant *out-of-phase* vehicle motions. The magnitude of the vehicle response in each mode is nearly equal to the ratio of the payload mass (or moment-of-inertia) to the appropriate *effective* vehicle mass or moment-of-inertia (i.e., including hull apparent mass and moment-of-inertia effects) for the dominant degree of freedom.

For example, consider the coupled heave vibration mode:

$$\left|w_{h_{c.g.}} : w_{p_{c.g.}}\right|_{\omega_{h_v}} = \left|0.179 : 1\right| \doteq \frac{\text{payload mass}}{\text{effective vehicle mass for } z\text{-axis motions}} = 0.175$$

These relatively high-frequency out-of-phase coupled modes could be important in the design and analysis of interelement structural members. Also, rotor excitation, including higher-order dynamics not modeled in the present simulation, could be significant at these frequencies.

The present example analysis of the coupled HLA/slung-load dynamics shows that while the characteristic roots of the separated vehicle (line b) and payload (line d) modes are essentially unchanged in the combined vehicle (lines c and e), significant dynamic coupling between the bodies exists. Adequate consideration of the coupled vehicle/slung-payload low-frequency modes will be essential for load positioning, and of the high-frequency modes for minimizing structural mode excitations. Analogous low-frequency problems with heavy-lift helicopters have required special flight control system characteristics, including feedbacks of the cable angle rates to rotor controls.[21] This remains an area for future HLA study.

The coupled vehicle/payload dynamics resemble in character the helicopter/slung-load results of Sampath.[18] However, the present payload aerodynamic model lacks the detail required to capture the oscillatory nonlinearities and stability sensitivities reported in that reference.

Effect of Flight Speed on Unloaded Vehicle Dynamics

The linearization analysis for the *unloaded* vehicle was extended over a range of trimmed flight speeds from 0 to 140 ft/s ($\alpha = 0$). The migration of the five modes with axial speed is shown in Fig. 6. The surge ($1/T_s$) and stable sway/yaw ($1/T_{sy_2}$) time constants increase fairly linearly with speed. The unstable sway mode time constant ($1/T_{sy_1}$) increases owing to the increasing hull instability with flight speed.

As expected from helicopter dynamics,[22] the heave damping ($1/T_h$) improves with increasing speed. Since both the rotor and tail effectiveness increase with speed, the roll mode becomes more stable, reaching a damping ratio of 0.53 at the flight speed of 140 ft/s. Forward flight speed reduces the frequency and ultimately destabilizes the pitch oscillation mode, due to the hull's large aerodynamic instability and the small tail area. However, the pitch damping of the rotors improves with increasing airspeed, so the mode is marginally stable up to 60 ft/s. At this speed, the dominance of the envelope aerodynamics over metacentric stability causes the oscillation to become unstable. Ultimately the mode becomes two aperiodic divergences as the speed further increases.

The sensitivity of the dynamic modes to forward flight speed is a very important consideration in configuration and flight control synthesis. The present analyses show the unaugmented, unloaded example HLA configuration to be best suited for low-speed and hover flight conditions ($V_0 < 60$ ft/s). Increased flight speed can be achieved by increasing the tail size and hull fineness ratio, or by incorporating an active stabilizing flight control system.

Comparison of Nonlinear and Decoupled Linear Models

Flight mechanics and control analyses commonly are based on the small perturbation, linearized dynamics of vehicle motion where the longitudinal (pitch, surge, and heave) and lateral (roll, yaw, and sway) degrees of freedom are assumed decoupled. The validity of employing such assumptions for

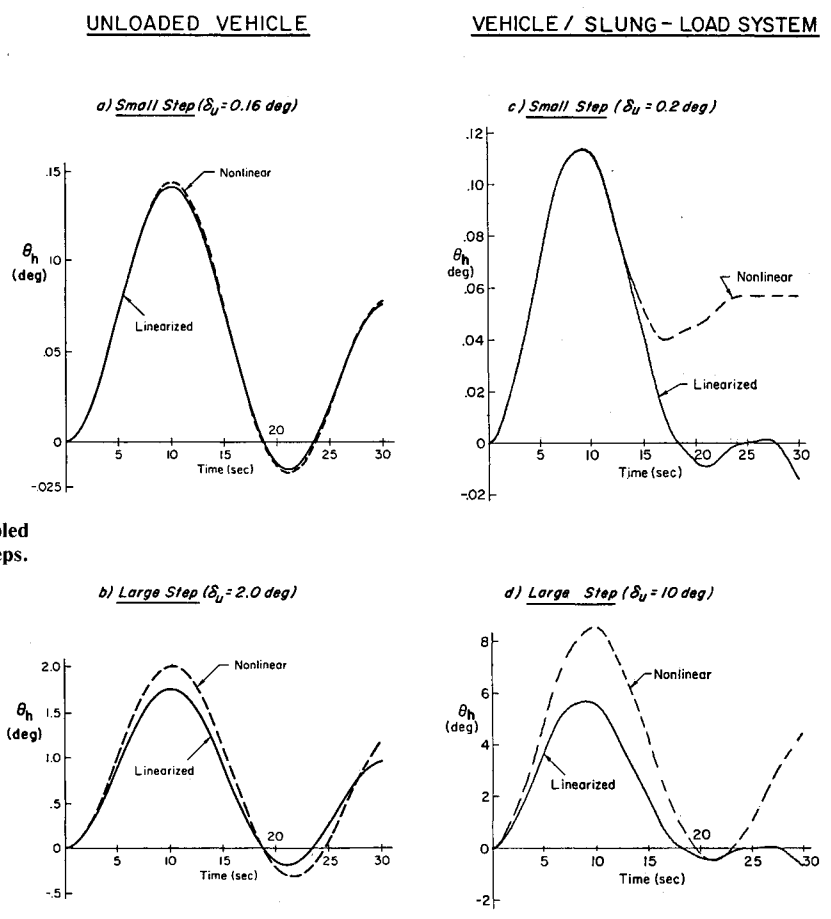

Fig. 7 Comparison of 6-DOF nonlinear and decoupled 3-DOF linear open-loop responses to axial control steps.

HLA analyses was checked by comparing the step response of the nonlinear and decoupled linear models for the 44-ft/s flight condition, with and without a slung payload.

Figure 7 shows the open-loop pitch attitude response of the vehicle to small and large step commands in surge control (δ_u).

The *unloaded* vehicle pitch angle in response to a small step command of surge control ($\delta_u = 0.16$ deg) is shown in Fig. 7a. The nonlinear and decoupled linear system responses compare very well, thereby validating the approximations. When the command is increased to $\delta_u = 2.0$ deg, Fig. 7b, the discrepancy between the system responses becomes more noticeable, indicating the existence of response nonlinearities for larger motions. However, the character of the response is well represented for this case where derivative discontinuities in the aerodynamic data for the tail (Fig. 2) are not encountered.

The 6DOF nonlinear and the decoupled 3DOF linear responses of the *vehicle/slung-payload* system are compared for a small command ($\delta_u = 0.2$ deg) and a large command ($\delta_u = 10.0$ deg) in Figs. 7c and 7d, respectively. During the first 15 s, the comparison is good, with the large command response exhibiting some nonlinearity, as before. Thereafter, the response of the linearized system diverges from the nonlinear system. This divergence was traced to the coupling between longitudinal and the lateral-directional degrees of freedom—a factor which is not represented in the decoupled linear model. As previously noted, the loaded vehicle exhibits significantly increased coupling due to the increased rotor flapping associated with the large trim thrust levels.

These results are typical for simulations of rotorcraft where substantial response nonlinearity and coupling between longitudinal- and lateral-directional degrees of freedom exists. The comparisons show that control and response coupling characteristics need to be taken into account in the analysis of HLA dynamics and the synthesis of flight control systems for these vehicles.

Vehicle Gust Response

The unloaded example configuration was trimmed at the 44-ft/s flight condition and then subjected to an isolated vertical tail gust in order to study the dynamic responses. The gust input was a one-minus-cosine shaped vertical downdraft with a maximum value of 5 ft/s and a duration of 4 s. The selection of an isolated tail gust (no hull gradients) was made in order to excite the vehicle pitch mode with a simple disturbance, not necessarily representative of a realistic gust environment.

Open-Loop Response

The longitudinal response of the open-loop vehicle to the tail gust input is shown in the solid time histories of Fig. 8. (Note that the rate of climb, $\dot{h}_{h_{c.g.}}$ not $w_{h_{c.g.}}$, is presented here.) The open-loop behavior is dominated by the pitch mode. The frequency of oscillation, phasing, and relative response ratios correspond very well, as expected, with the previous linearized results.

Closed-Loop Response

The flight control system was closed in all 6-deg of hull freedom in order to compare open- and closed-loop unloaded vehicle response to the gust input. Details of the pitch loop closure were presented in Ref. 11.

The longitudinal closed-loop response to the tail down gust is plotted (dotted lines) in Fig. 8. The disturbance-suppressing characteristics of the 6DOF flight control system are clearly apparent. Further studies are needed to determine vehicle response to turbulent environments, utilizing the four-point-gust model[11] with realistic turbulence inputs and the aerodynamic interference models.[13]

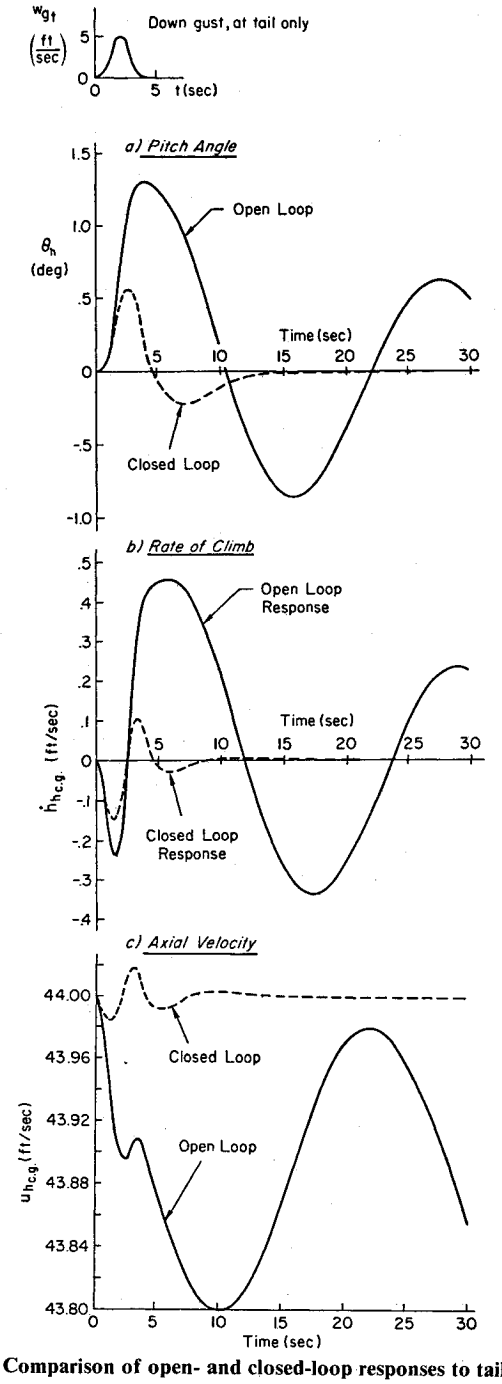

Fig. 8 Comparison of open- and closed-loop responses to tail-down gust.

IV. Conclusions

An example HLA configuration with a low fineness ratio hull and a small vee-tail was analyzed to expose basic aerodynamic and dynamic properties. Some of the significant conclusions to be drawn from this analysis and a comparison with past airship data follow:

1) For the example configuration, the tail size is not sufficient to stabilize the vehicle in cruise flight.

2) The choice and scheduling of control mixing between rotors and propellers has a significant effect on vehicle performance. For the example configuration, the loaded and unloaded vehicles exhibited about the same maximum speed because the fixed crossfeed values resulted in higher propulsive efficiency for the loaded condition.

3) The trimming capability of the unloaded HLA is severely limited when hovering in crosswinds owing to lack of lateral force generation capability.

4) Numerically linearized small perturbation dynamic analysis of the unloaded example configuration showed the existence of five characteristic response modes: surge subsidence (stable); heave subsidence (stable); pitch oscillation (stable); coupled sway-yaw (unstable); and roll oscillation (stable). Resemblance of some of the HLA modes to those of classical aircraft and V/STOLs is apparent. The qualitative correlation of these modes with the results of other investigators was noted.

5) Analysis of the vehicle/slung-payload dynamics shows significant coupling of the payload dynamics with those of the basic HLA.

6) The pitch and unstable sway-yaw (unloaded vehicle) modes were destabilized with increasing axial flight speed, while the other modes became more stable.

7) Comparison of nonlinear and decoupled linear solutions for the unloaded vehicle showed close agreement for small motions, with some nonlinear effects for motions larger than a few degrees. The loaded vehicle exhibits strongly coupled characteristics due to the rotor flapping dynamics.

8) Open- and closed-loop responses of a 5 ft/s (one-minus-cosine) down gust on the tail showed that excellent improvement in the vehicle's dynamic behavior can be attained with the incorporation of simple flight controller having proportional, rate and integral-error feedbacks.

Acknowledgments

The work reported herein was sponsored by the National Aeronautics and Space Administration under Contract NAS2-10330, with Mark Ardema, Alan Faye, and Peter Talbot as Contract Technical Monitors.

References

[1] Ardema, M.D., "Vehicle Concepts and Technology Requirements for Buoyant Heavy-Lift Systems," SAE Paper 791090, 1979.

[2] Piasecki, F.N., "Ultra Heavy Vertical Lift System—The 'Helistat'," *Interagency Workshop on Lighter Than Air Vehicles,* MIT, FTL R75-2, Jan. 1975.

[3] "Feasibility Study of Modern Airships. Phase II: Executive Summary," Goodyear Aircraft Co., NASA CR-2922, Nov. 1977.

[4] Delaurier, J. and Schenck, D., "Airship Dynamic Stability," AIAA Paper 79-1591, 1979.

[5] Nagabhushan, B.L. and Tomlinson, N.P., "Flight Dynamics Analyses and Simulation of Heavy Lift Airships," AIAA Paper 79-1593, 1979.

[6] Nielsen, J.N., McMillan, O.J., Spangler, S.B., Woolley, J.P., "Feasibility Study of Modern Airships. Phase II, Vol. I: Heavy Lift Airship Vehicle. Book III: Aerodynamic Characteristics of Heavy Lift Airship as Measured at Low Speeds," NASA CR-151919, Sept. 1976.

[7] Spangler, S.B. and Smith, C.A., "Theoretical Study of Hull-Rotor Aerodynamic Interference on Semibuoyant Vehicles," NASA CR-152127, April 1978.

[8] Flomenhoft, H.I., "Gust Loads on Airship Fins," McLean Development Laboratories, E-114, June 1957.

[9] Calligeros, J.M. and McDavitt, P.W., "Response and Loads on Airships Due to Discrete and Random Gusts," MIT, Cambridge, Mass., ASRL TR 72-1, Feb. 1958.

[10] Curtiss, H.C. Jr., Hazen, D.C., and Putman, W.F., "LTA Aerodynamic Data Revisited," AIAA Paper 75-951, July 1975.

[11] Tischler, M.B., Jex, H.R., and Ringland, R.F., "Simulation of Heavy Lift Airship Dynamics over Large Ranges of Incidence and Speed," AIAA Paper 81-1335, July 1981.

[12] Ringland, R.F., Tischler, M.B., Ashkenas, I.L., Jex, H.R., "Generic Multi-Body Formulation of Heavy-Lift Airship Equations of Motion," *Proceedings of the Joint Automatic Control Conference,* Vol. I, San Francisco, Aug. 1980.

[13] Tischler, M.B., Ringland, R.F., Jex, H.R., and Ashkenas, I.L., "Flight Dynamics Analysis and Simulation of Heavy Lift Airships," Systems Technology, Inc., TR 1151-2-II, 1982.

[14] Hoerner, S.F., *Fluid Dynamic Lift,* published by author, 1975.

[15] Hoerner, S.F., *Fluid Dynamic Drag,* published by author, 1965.

[16]Dempsey, E.M., "Static Stability Characteristics of a Systematic Series of Stern Control Surfaces on a Body of Revolution," DWT HSRDC Report 77-0085, 1977.

[17]Humphreys, D.E. and Watkinson, K.W., "Prediction of Acceleration Hydrodynamic Coefficients for Underwater Vehicles from Geometric Parameters," NCSL TR 327-78, Feb. 1978.

[18]Sampath, Prasad, "Dynamics of a Helicopter-Slung Load System," Ph.D. thesis, University of Maryland, College Park, Md., 1980.

[19]Hoh, R.H. and Ashkenas, I.L., "Development of VTOL Flying Qualities Criteria for Low Speed and Hover," NADC 77052-30, Dec. 1979.

[20]McRuer, D., Ashkenas, I., and Graham, D., *Aircraft Dynamics and Automatic Control,* Princeton University Press, Princeton, N.J., 1973.

[21]Fries, G.H. and Schneider, J.J., "HLH and Beyond," SAE Paper 791086, Dec. 1979.

[22]Bramwell, A.R.S., *Helicopter Dynamics,* John Wiley and Sons, New York, 1976.